



# Influence of pouring temperature on solidification behavior, microstructure and mechanical properties of sand-cast Mg–10Gd–3Y–0.4Zr alloy

Song PANG<sup>1,2</sup>, Guo-hua WU<sup>1</sup>, Wen-cai LIU<sup>1</sup>, Liang ZHANG<sup>1</sup>, Yang ZHANG<sup>1</sup>, Hans CONRAD<sup>2</sup>, Wen-jiang DING<sup>1</sup>

1. National Engineering Research Center of Light Alloy Net Forming and

State Key Laboratory of Metal Matrix Composite, Shanghai Jiao Tong University, Shanghai 200240, China;

2. Department of Materials Science and Engineering, North Carolina State University, Raleigh, NC 27695-7907, USA

Received 21 March 2014; accepted 21 July 2014

**Abstract:** Influence of the pouring temperature ranging from 680 to 780 °C on the solidification behavior, the microstructure and mechanical properties of the sand-cast Mg–10Gd–3Y–0.4Zr alloy was investigated. It was found that the nucleation undercooling of the  $\alpha$ -Mg phase increased from 2.3 to 6.3 °C. The average  $\alpha$ -Mg grain size increased from 44 to 71  $\mu\text{m}$ , but then decreased to 46  $\mu\text{m}$ . The morphology of the eutectic compound transformed from a continuous network into a discontinuous state and then subsequently into an island-like block. The volume fraction of  $\beta$ -Mg<sub>24</sub>RE<sub>5</sub> phase increased and its morphology transformed from particle into rod-like. The increase in pouring temperature increased the solute concentration. YS increased from 138 to 151 MPa, and UTS increased from 186 to 197 MPa. The alloy poured at 750 °C had optimal combining strength and ductility. The fracture surface mode transformed from quasi-cleavage crack into transgranular fracture, all plus the dimple-like fracture, with the micro-porosity and the re-oxidation inclusion as major defects. The average  $\alpha$ -Mg grain size played a main role in the YS of sand-cast Mg–10Gd–3Y–0.4Zr alloy, besides other factors, i.e. micro-porosity, morphology of eutectic compounds, re-oxidation inclusion and solute concentration.

**Key words:** sand-cast; Mg alloys; solidification; microstructure; mechanical properties

## 1 Introduction

Mg-based alloys with rare earth (RE) elements addition have attracted attention as light structural materials due to their low density, high strength, good creep resistance and high damping capacities [1–3]. Zirconium-refined rare earth magnesium alloys (Mg–RE–Zr) have recently been developed and studied, such as Mg–RE–Zn (ZE) [4], Mg–RE–Y (WE) [5], Mg–Nb–Zn (NZ) [6] and Mg–Gd–Y (GW) [7]. The results [8–10] show that the Mg–10Gd–3Y–0.4Zr (GW103) alloy exhibits a combination of strength and ductility among rare earth magnesium alloys.

Mechanical properties of cast alloys are based on their as-cast microstructure, which depends on cooling rate, pouring temperature, nucleation sites and temperature gradient during solidification [11]. As an essential thermodynamic parameter, the pouring temperature has a significant influence on the final

as-cast microstructure of the alloy, including the grain size, the morphology of the eutectic phase, and the distribution of solutes [12–16]. The pouring temperature is also considered a major parameter of the sand-cast process, especially for forming extremely complex castings in the aerospace industry. There are some researches related to the microstructure and mechanical properties of sand-cast GW103K alloys. But most of them only focused on the influence of the precipitation on the mechanical properties of alloys after heat treatment [17–20]. Thus, the aim of this study is to investigate the influence of the pouring temperature on the solidification behavior, the microstructure and mechanical properties of the sand-cast GW103K alloy.

## 2 Experimental

Sand-cast Mg–10Gd–3Y–0.4Zr (mass fraction, %) alloy (GW103K) was employed in the present study. High purity Mg (99.95%) ingots, and Mg–25Gd (mass

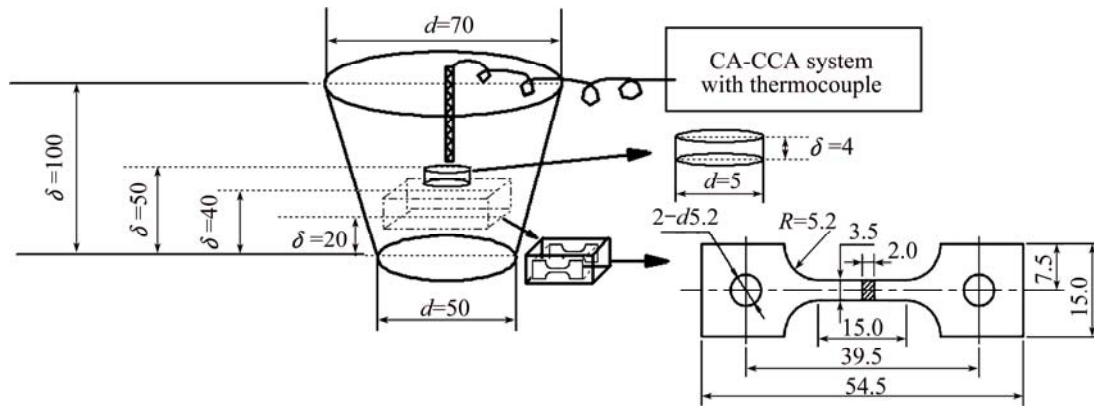


**Fig. 1** Location and dimensions of thermocouple and specimen for microstructure observation and mechanical property test (unit: mm)

fraction, %), Mg–25Y (mass fraction, %) and Mg–30Zr (mass fraction, %) master alloys were used. The melting process was carried out in an electric resistance furnace under the mixed atmosphere of CO<sub>2</sub> and SF<sub>6</sub> with the volume ratio of 100:1. After being refined at 750 °C the alloy melt was first held at 780 °C for 10 min, then cooled to the pouring temperature and poured into a sand cup. Figure 1 shows the schematic of the casting, the location of K type thermocouples, and the location and dimensions of the specimen for the microstructure observation and the mechanical property test.

The chemical composition of alloys was determined by an inductively coupled plasma analyzer (Perkin Elmer, Plasma–400), and the results are listed in Table 1. During the solidification, the time and temperature were recorded by a self-assembly computer-aided cooling curve analysis (CA-CCA) system with K-type thermocouples. The analysis process included smoothing, curve fitting, plotting the first derivatives, identifying the onset and end of solidification, determining solidification parameters such as, cooling rate, nucleation temperatures, nucleation undercooling, and growth temperature [21–23]. Details of the cooling process and related solidification parameters are shown in Fig. 2 and Table 2. The specimen for microstructure observation was successively ground using SiC papers, polished using diamond suspensions and MgO particles solution, and etched in a solution of HNO<sub>3</sub> (4% in volume fraction) and alcohol. Then, the microstructure observation was

**Table 1** Chemical composition of sand-cast GW103K alloys poured at different pouring temperatures

Temperature/°C	Mass fraction/%			
	Gd	Y	Zr	Mg
680	10.39	2.32	0.35	Bal.
720	10.32	2.42	0.32	Bal.
750	10.36	2.34	0.31	Bal.
780	10.43	2.26	0.32	Bal.

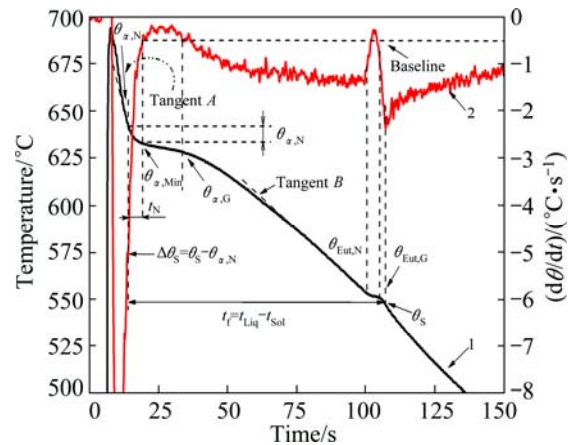


**Fig. 2** Cooling curve (line 1), the first derivative curve (line 2) and representation of characteristic parameters used in present study for sand-cast GW103K alloy

**Table 2** Solidification characteristic parameters identified during solidification of sand-cast GW103K alloys by thermal analysis

Characteristic symbol	Characteristic description
$\theta_{\alpha,N}$	$\alpha$ -Mg nucleation temperature (liquidus)
$\theta_{\alpha,Min}$	$\alpha$ -Mg minimum temperature
$\Delta\theta_N$	Nucleation undercooling ( $\Delta\theta_N = \theta_{\alpha,N} - \theta_{\alpha,Min}$ )
$t_{\alpha,N}$	Nucleation undercooling time
$\theta_{\alpha,G}$	$\alpha$ -Mg dendrite growth temperature
$\theta_{Eut,N}$	Eutectic nucleation temperature
$\theta_{Eut,G}$	Eutectic growth temperature
$\theta_S$	Solidus temperature (end of solidification process)
$\Delta\theta_S$	Solidification temperature range ( $\Delta\theta_S = \theta_{\alpha,N} - \theta_S$ )
$t_f$	Total solidification time

performed with optical microscope (OM) and scanning electron microscope (SEM, FEI SIRION 200/INCA OXFORD). The average  $\alpha$ -Mg grain size was measured

by the linear intercept technique (ASTM 112–96). Five fields were considered for each measurement with approximately 60 intercepts in each field. The composition and distribution of the elements were determined by the energy dispersive spectroscope (EDS) attached to the SEM. The tensile properties were determined at room temperature on the sheet-shaped specimens at the initial strain rate of  $5 \times 10^{-4} \text{ s}^{-1}$  with a Zwick/Roell Z020 tensile machine.

### 3 Results and discussion

#### 3.1 Solidification behavior

Figure 3 shows the cooling curves and the first derivatives of the sand-cast GW103K alloys at different pouring temperatures. The solidification process of the studied alloys included two reactions: 1)  $L \rightarrow \alpha\text{-Mg}$ , and 2)  $L \rightarrow \text{Mg} + \beta\text{-Mg}_{24}\text{RE}_5$ . The related characteristic parameters are listed in Table 3 and Table 4.

##### 3.1.1 Solidification parameters of $\alpha\text{-Mg}$ phase

Figure 4 shows the relationships between the pouring temperature ( $\theta_p$ ) and solidification parameters of the  $\alpha\text{-Mg}$  phase, including nucleation temperature, minimum temperature and growth temperature of the

$\alpha\text{-Mg}$  phase. The results showed that both the nucleation temperature and the growth temperature of the  $\alpha\text{-Mg}$  phase increased, but the minimum temperature first fluctuated between 633.4 °C and 633.9 °C but then decreased to 631.7 °C when the pouring temperature increased from 680 °C to 780 °C. There were three polynomial relationships related to the influence of the pouring temperature on these solidification parameters ( $\theta_{\alpha,N}$ ,  $\theta_{\alpha,\text{Min}}$  and  $\theta_{\alpha,G}$ ) of the  $\alpha\text{-Mg}$  phase, respectively. The empirical fitting functions are

$$\theta_{\alpha,N} = 628.89 + 0.20\theta_p - 0.0009\theta_p^2, R^2 = 0.997 \quad (1)$$

$$\theta_{\alpha,\text{Min}} = 629.19 + 0.03\theta_p - 0.0003\theta_p^2, R^2 = 0.994 \quad (2)$$

$$\theta_{\alpha,G} = 630.04 + 0.06\theta_p - 0.0003\theta_p^2, R^2 = 0.978 \quad (3)$$

##### 3.1.2 Undercooling behavior

Figure 5 shows the influence of pouring temperature on the nucleation undercooling parameters ( $\Delta\theta_N$  and  $\Delta t_N$ ) of the  $\alpha\text{-Mg}$  phase. With the increase in pouring temperature from 680 °C to 750 °C, the nucleation temperature of the  $\alpha\text{-Mg}$  phase increased from 2.3 °C to 6.3 °C, but did not increase with further increase in pouring temperature up to 780 °C. Meanwhile, the nucleation time of the  $\alpha\text{-Mg}$  phase increased but then

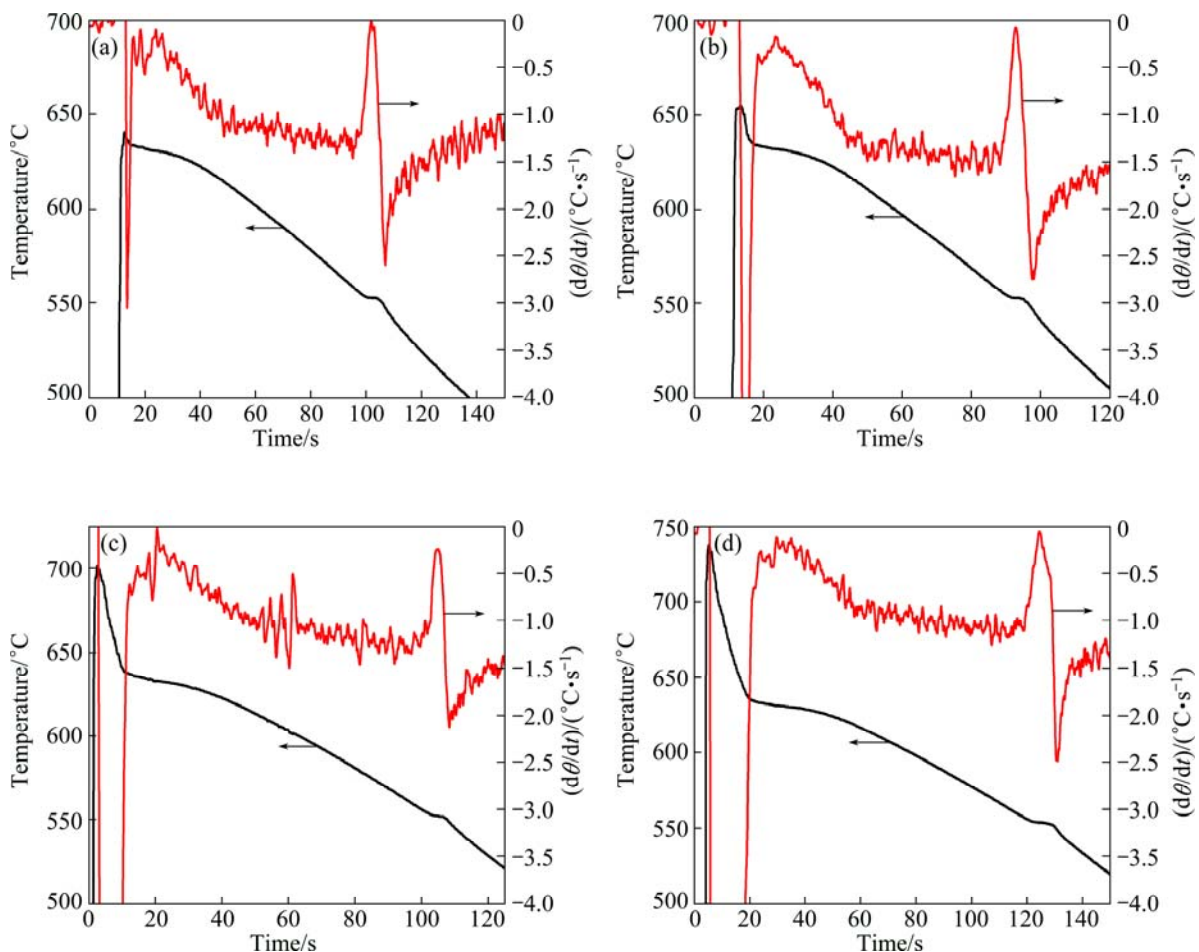


**Fig. 3** Cooling curves and the first derivative curves of sand-cast GW103K alloys at different pouring temperatures: (a) 680 °C; (b) 720 °C; (c) 750 °C; (d) 780 °C

**Table 3** Solidification characteristic parameters of  $\alpha$ -Mg phase of sand-cast GW103K alloys poured at different temperatures

$\theta_p/^\circ\text{C}$	$\theta_{\alpha,N}/^\circ\text{C}$	$\theta_{\alpha,G}/^\circ\text{C}$	$\theta_{\alpha,\text{Min}}/^\circ\text{C}$	$\Delta\theta_{\alpha,N}/^\circ\text{C}$	$t_{\alpha,N}/\text{s}$
680	634.0	630.0	631.7	2.3	4.08
720	638.7	630.3	633.4	5.3	7.52
750	639.9	630.1	633.6	6.3	8.96
780	640.2	629.3	633.9	6.3	6.65

**Table 4** Eutectic reaction temperatures and other solidification parameters of sand-cast GW103K alloys poured at different temperatures

$\theta_p/^\circ\text{C}$	$\theta_{\text{Eut},N}/^\circ\text{C}$	$\theta_{\text{Eut},G}/^\circ\text{C}$	$\Delta\theta_s/^\circ\text{C}$	$t_s/\text{s}$	$\theta_s/^\circ\text{C}$	CR/ $(^\circ\text{C}\cdot\text{s}^{-1})$
680	554.1	552.4	86.3	82.0	547.7	2.63
720	554	552.4	90.6	89.3	548.1	2.5
750	554.3	552.1	91.5	98.3	548.4	2.33
780	554.2	552.5	101.4	112.7	548.8	2.25

Note: CR stands for the cooling rate, which is determined with the formula  $CR=(\theta_{\text{liq}}-\theta_{\text{sol}})/(t_{\text{liq}}-t_{\text{sol}})$ , where  $\theta_{\text{liq}}$  and  $\theta_{\text{sol}}$  are the liquidus and solidus temperatures, and  $t_{\text{liq}}$  and  $t_{\text{sol}}$  are the time from the cooling curve that corresponds to liquidus temperature ( $\theta_{\alpha,N}$ ) and solidus temperature ( $\theta_s$ ), respectively.

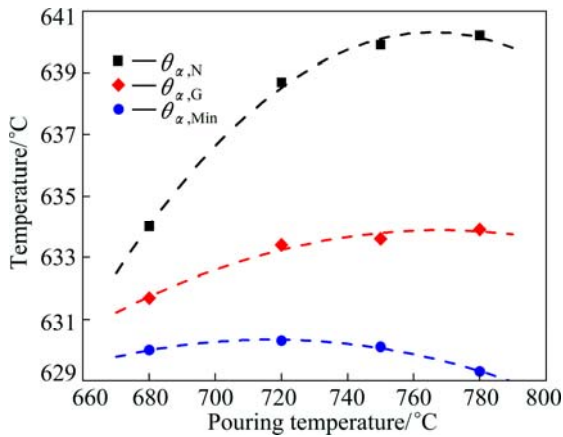


**Fig. 4** Effect of pouring temperature on solidification parameters of  $\alpha$ -Mg phase of sand-cast GW103K alloys

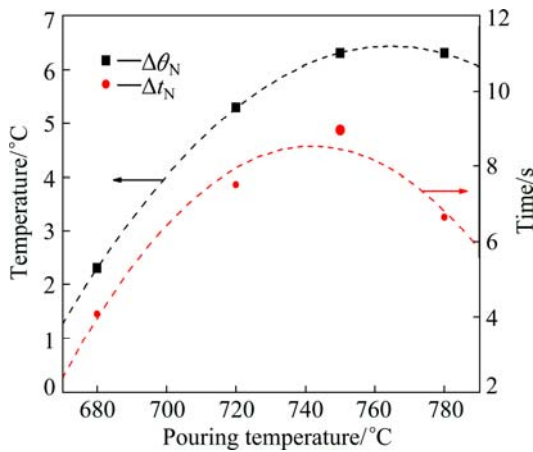


**Fig. 5** Effect of pouring temperature on nucleation undercooling parameters of  $\alpha$ -Mg phase ( $\Delta\theta_N$  and  $\Delta t_N$ ) of sand-cast GW103K alloys

decreased at the pouring temperature of 750 °C. The empirical fitting functions are

$$\Delta\theta_N = -1.52 + 0.22\theta_p - 0.0012\theta_p^2, R^2 = 0.962 \quad (4)$$

$$\Delta t_N = -1.15 + 0.13\theta_p - 0.0006\theta_p^2, R^2 = 0.956 \quad (5)$$

3.1.3 Solidification temperature range and cooling rate

Figure 6 shows the influence of the pouring temperature on the eutectic reaction temperature and the solidus temperature. It indicated that the pouring temperature could affect the solidus temperature, but had no significant influence on the eutectic reaction. There is a linear relationship between  $\theta_s$  and  $\theta_p$ , and the empirical fitting function is

$$\theta_s = 547.35 + 0.01\theta_p, R^2 = 0.995 \quad (6)$$

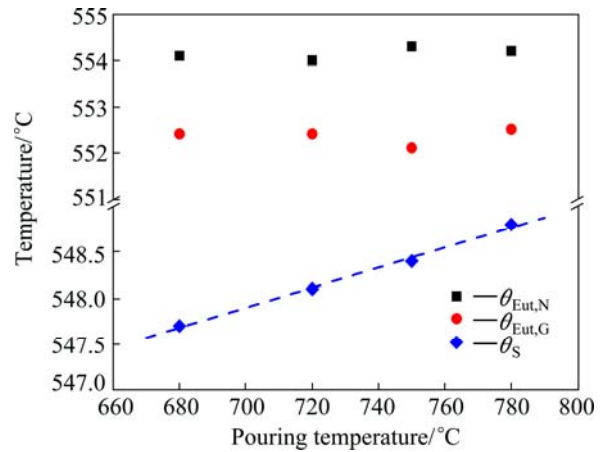


**Fig. 6** Effect of pouring temperature on eutectic reaction temperatures ( $\theta_{\text{Eut},N}$  and  $\theta_{\text{Eut},G}$ ) and solidus temperature ( $\theta_s$ ) of sand-cast GW103K alloys

Figure 7 shows the influence of the pouring temperature on solidification temperature range ( $\Delta\theta_s$ ) and time range ( $\Delta t_s$ ) of sand-cast GW103K alloys, both of which increased with increase in pouring temperature. The empirical fitting functions are

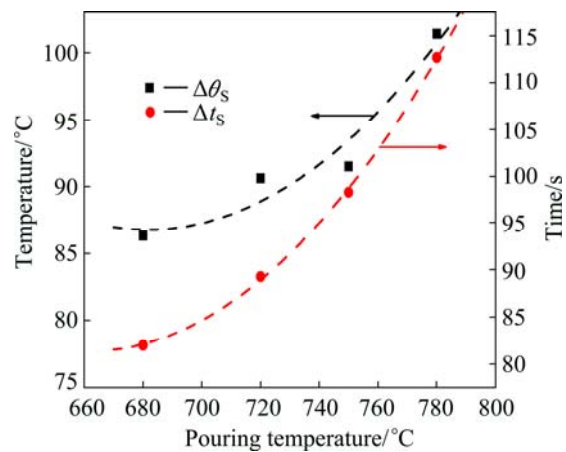


**Fig. 7** Effect of pouring temperature on solidification temperature range ( $\Delta\theta_s$ ) and time range ( $\Delta t_s$ ) of sand-cast GW103K alloys

$$\Delta\theta_s=88.20-0.09\theta_p-0.0014\theta_p^2, R^2=0.938 \quad (7)$$

$$\Delta t_s=81.66-0.05\theta_p-0.0022\theta_p^2, R^2=0.999 \quad (8)$$

Another thermodynamic parameter, the cooling rate (CR), was also significantly affected by the pouring temperature, which decreased with increase in pouring temperature (Fig. 8). There is a linear relationship between CR and  $\theta_p$ , which is given by

$$CR=2.75-0.004\theta_p, R^2=0.983 \quad (9)$$

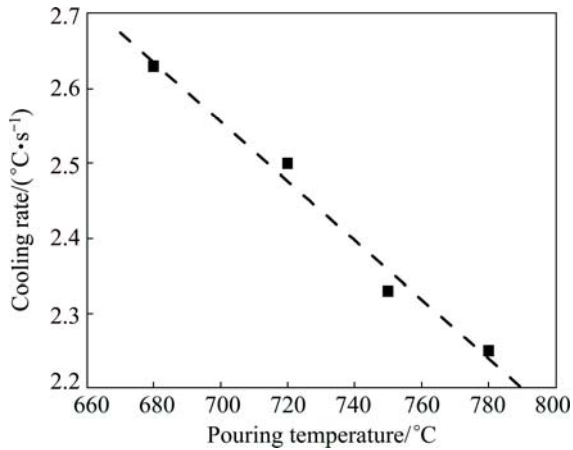


**Fig. 8** Effect of pouring temperature on cooling rate of sand-cast GW103K alloys

### 3.2 Metallographic characteristics

#### 3.2.1 Grain size

The optical microstructure of sand-cast GW103K alloys poured at different temperatures consisted of

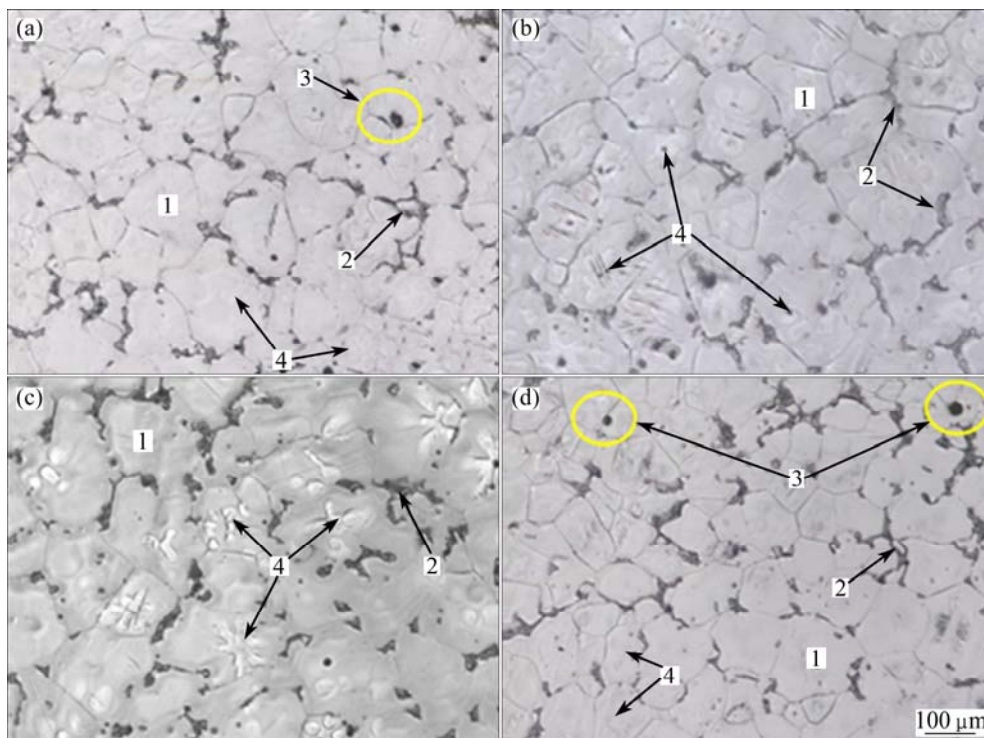
equiaxed  $\alpha$ -Mg matrix, eutectic compounds along the grain boundaries and some inclusions (Fig. 9). Point 4 in most  $\alpha$ -Mg grains presented some petal-like cores, which were proved to be zirconium clusters in Refs. [3,5,10,24].

Figure 10 shows that the average  $\alpha$ -Mg grain size ( $d$ ) increased from 44  $\mu\text{m}$  to 71  $\mu\text{m}$ , and then sharply decreased to 46  $\mu\text{m}$  with the pouring temperature ranging from 680  $^{\circ}\text{C}$  to 780  $^{\circ}\text{C}$ . The polynomial relationship between  $d$  and  $\theta_p$  is given by

$$d=1.48+1.69\theta_p-0.0103\theta_p^2, R^2=0.969 \quad (10)$$

#### 3.2.2 Eutectic phase

Besides the average  $\alpha$ -Mg grain size, increase in pouring temperature had a significant influence on the morphology of the eutectic compound, transforming from a continuous network first into a separated state (Fig. 9(a) and Fig. 11(a)) and then into an island-like block (Fig. 9(d) and Fig. 11(c)). Furthermore, the size of the eutectic compound became larger with increase in pouring temperature. The energy-dispersive X-ray analysis (EDS) results of sand-cast GW103K alloys poured at different pouring temperatures are shown in Figs. 11(b) and (d). The bright region volume ratio in Fig. 11(c) was higher than Fig. 11(a), which had been proven to consist of the  $\beta$ -Mg<sub>24</sub>RE<sub>5</sub> phase and supersaturated solid solution of rare earth elements in our previous work [7]. There was almost no visible  $\beta$ -Mg<sub>24</sub>RE<sub>5</sub> phase observed within the eutectic phase of the alloy poured at 680  $^{\circ}\text{C}$  in Fig. 11(a). However, as the pouring



**Fig. 9** Optical microstructures of sand-cast GW103 alloys at different pouring temperatures: (a) 680  $^{\circ}\text{C}$ ; (b) 720  $^{\circ}\text{C}$ ; (c) 750  $^{\circ}\text{C}$ ; (d) 780  $^{\circ}\text{C}$  (1— $\alpha$ -Mg matrix; 2—Mg—Mg<sub>24</sub>RE<sub>5</sub> eutectic compound; 3—Inclusion; 4—Zirconium cluster)

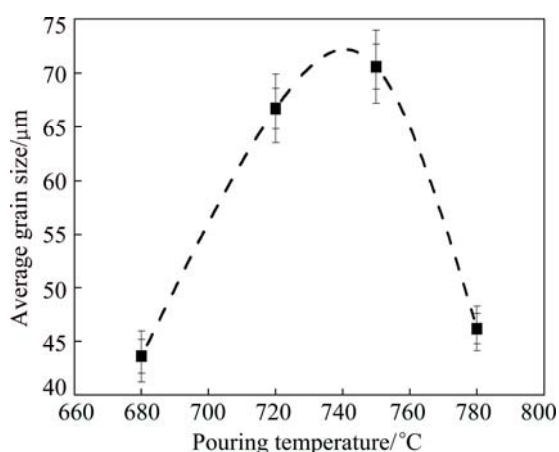


**Fig. 10** Effect of pouring temperature on average  $\alpha$ -Mg grain size of sand-cast GW103K alloys

temperature increased up to 780 °C, a large amount of  $\beta$ -Mg<sub>24</sub>RE<sub>5</sub> particles occurred, and some rod-like  $\beta$ -Mg<sub>24</sub>RE<sub>5</sub> particles appeared in the eutectic phase in Fig. 11(c). Results of EDS showed that both areas 1 and 2 were the supersaturated solid solution rich in Gd, Y and Zr. Furthermore, all solute contents in area 2 were higher than those in area 1. This indicated that the increase in pouring temperature increased the solute content in the supersaturated solid solution.

### 3.3 Mechanical properties

The influence of the pouring temperature on the yield strength (YS), the maximum strength (UTS) and elongation (El) is presented in Fig. 12. With increase in the pouring temperature from 680 °C to 780 °C, the YS increased from 138 MPa to 151 MPa, and the UTS increased from 186 MPa to 197 MPa. The elongation first increased, but then decreased with the highest value of 2.4%. The alloy poured at 750 °C showed the optimal combined strength and ductility.

## 4 Discussion

### 4.1 Solidification kinetics

The characteristic parameters of metallurgical reactions during solidification can be determined by computer aided cooling curve analysis method (CA-CCA). This approach can provide the relative kinetics data pertaining to the solidification process as a function of the pouring temperature in the present study.

In the casting process, the pouring temperature is always higher than the liquidus of the metal, which is believed to be above the critical temperature described as “quasi-real solution”, where only few clusters or crystalline particles exist [25]. The critical temperature is based on the factors related to the liquid metal including

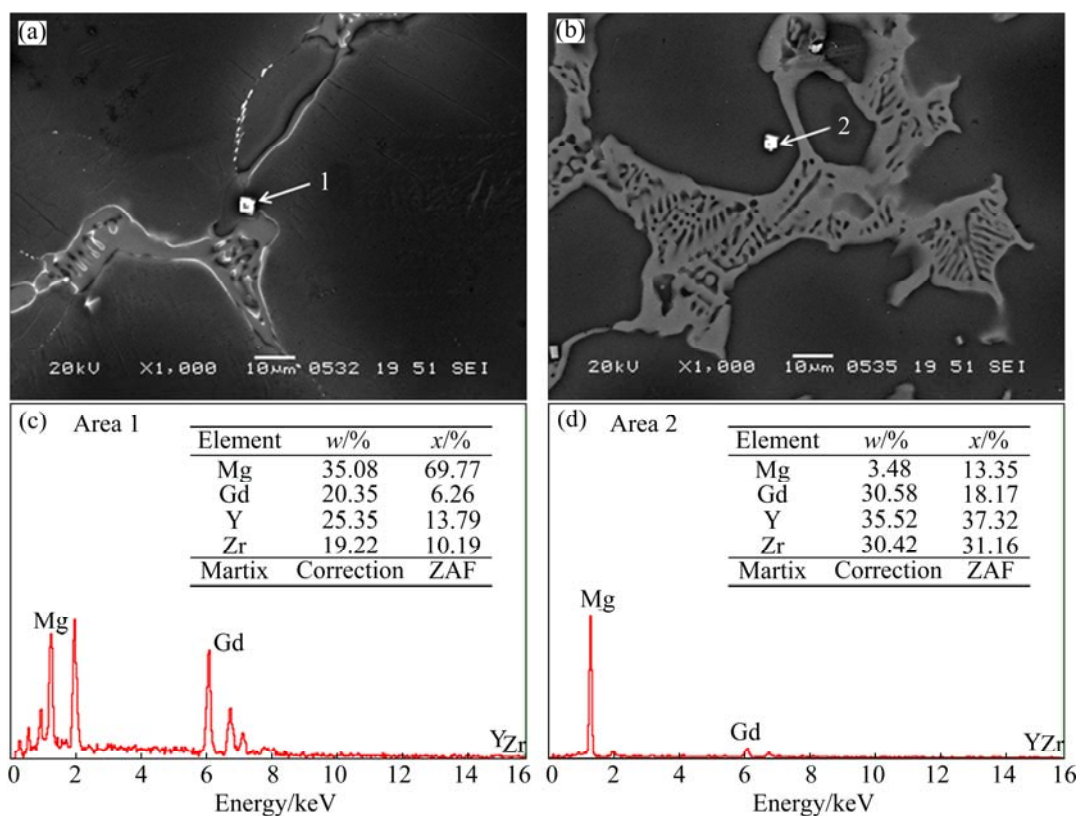


**Fig. 11** Microstructures and EDS results of sand-cast GW103K alloys at different pouring temperatures: (a) 680 °C; (b) 780 °C; (c) Corresponding EDS analysis for area 1; (d) Corresponding EDS analysis for area 2

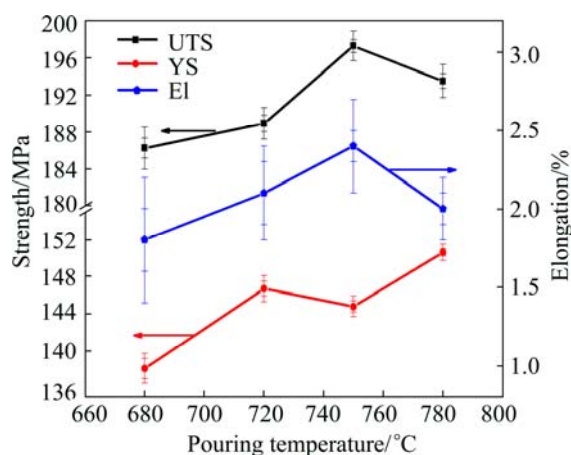


**Fig. 12** Effects of pouring temperature on tensile properties of sand-cast GW103K alloys

chemical composition, crystal structure, etc [26]. A higher pouring temperature gives a higher temperature difference between the pouring temperature and the critical temperature, and thereby enhances the driving force for the nucleation of solidification. This is why the nucleation temperature of the  $\alpha$ -Mg phase increased with increase in the pouring temperature. Although nucleation and growth of the  $\alpha$ -Mg phase occur at the same time, the minimum temperature has been proven to be the special parameter which divides the forming of the  $\alpha$  phase into two stages: main nucleation and main growth [22]. It was shown that the minimum temperature first fluctuated between 633.4 °C and 633.9 °C but then decreased to 631.7 °C (Fig. 4). The fluctuated minimum temperature cannot be the direct evidence for the influence of the pouring temperature on the nucleation. However, the decrease in fluctuated minimum temperature indicated that the nucleation process was extended, when there was a 1.7 °C decrease in minimum temperature of the  $\alpha$ -Mg phase poured at 780 °C.

There was no significant recalescence, due to the studied alloy itself and the solidification condition in the present study. According to solidification theory, the growth temperature of the  $\alpha$ -Mg phase is considered the end of the growth, which is also the recalescence point [11,26]. With the effective grain refiner zirconium, there are a number of critical nuclei, which are too small to allow the release of the latent heat of molten metal. Thus, the alloy undercools until the nuclei have grown and heat release can catch up with the removal and restore the balance that leads to the horizontal part of the cooling curve [22]. A high pouring temperature brings a high thermal input, which extends the balancing time, as shown in Fig. 3.

Figure 6 shows that there are no obvious differences in the eutectic reaction temperatures  $\theta_{\text{Eut,N}}$  and  $\theta_{\text{Eut,G}}$ . This can be explained through the basis of the constitutional

supercooling combined with undercooling. The coupled zone is an area on the phase diagram defining composition at the very temperature where the two eutectic phases can grow with the similar velocity [11]. Different composition brings different constitutional supercooling, which disturbs the formation of the eutectic phases. Due to the approximately same chemical composition of the GW103K alloys in the present study, there was no clear difference in the coupled zone, or any significant constitutional supercooling. It was shown that the cooling rate decreased from 2.65 °C/s to 2.25 °C/s with increase in the pouring temperature in Fig. 7. However, this little difference about 0.4 °C/s cannot have a significant influence on the eutectic reaction process, as indicated in Fig. 3 and Fig. 6. As a result, increase in pouring temperature had no identifying influence on the shift of the eutectic point which ranged from 680 °C to 780 °C. It was also shown that the solidus temperature increased with the increase in pouring temperature in Fig. 6. The number of the critical nucleus increased with the increase in the difference between the pouring temperature and the mold temperature [11], accelerating the consumption of the liquid in the solidification system, and in turn the formation of solid zone [26,27].

#### 4.2 Grain refinement

The nucleation undercooling and nucleation time of the  $\alpha$ -Mg phase increased, when the pouring temperature increased from 680 °C to 750 °C. According to the classical solidification theory [11,26]. This would cause an increase in the number of nuclei, which resulted in grain refinement in the as-cast microstructure of the alloy. The nucleation undercooling did not increase any more while the nucleation time decreased, when the pouring temperature was 780 °C. The increase in number of the nuclei would cause a decrease in the average  $\alpha$ -Mg grain size.

However, the average grain size of  $\alpha$ -Mg in Fig. 9 is totally different from the predicted result. The number of the critical nuclei was supposed to be a factor for this. When the temperature of the liquid metal was below the critical temperature, the critical nucleus formed and subsequently transformed into clusters or crystalline particles [22,25]. This explosive manner of nucleation has been termed as “Big Bang” nucleation by CHALMERS [28]. A large nucleation rate is a necessary condition for grain refinement, but not a sufficient one on its own. The final effect of grain refinement is also dependent on the survival rate of the nuclei produced by the “Big Bang” nucleation. In the conventional casting process, overheated liquid metal is poured into the relatively cold mould. Heterogeneous nucleation takes place immediately in the undercooled liquid close to the mould wall. The majority of the nuclei are transferred by

the convection caused by mould filling to the overheated liquid region and dissolved; only some of the nuclei survive and contribute to the final microstructure. But these could probably be re-melted by the extra heat [26], and as a result, the survival number of critical nuclei can be given by  $N_{\text{survival}}=N_{\text{formed}}-N_{\text{re-melted}}$ , where  $N_{\text{survival}}$  is the survival number of the critical nuclei,  $N_{\text{formed}}$  is the formed number of the critical nuclei, and  $N_{\text{re-melted}}$  is the re-melted number of the critical nuclei. The cooling rate was supposed to be the other factor. With the pouring temperature increasing from 680 °C to 750 °C, the corresponding cooling rate decreased from 2.65 °C/s to 2.25 °C/s. The decrease in the cooling rate caused the increase in the solidification time, which could probably extend the growth time of the  $\alpha$ -Mg phase. These two factors could be used to explain why the average grain size of the  $\alpha$ -Mg phase did not decrease, but increased, when nucleation undercooling increased with increase in the pouring temperature from 680 °C to 750 °C.

Furthermore, the superheating of the molten metal was over 130 °C, when the pouring temperature increased up to 780 °C, considering the melting point of the studied alloy below 650 °C [7]. Based on the fact that the residual covalent bonds exist in the liquid metal, namely the short range order, the molten metal has different structures at different temperatures [29,30]. A proper superheating over 100 °C can significantly change the structure and the atom clusters of the molten metal by increasing the number of the active atom clusters, which are responsible for the critical nuclei and in turn the formed nuclei [26]. IL'INSKII et al [31] pointed out that the number of clusters was higher with their size smaller and the activation energy was lower at a related higher temperature, studying on the structure of liquid which consists of atomic clusters and a proportion of free atoms filling the space between clusters above the melting point. An increase in pouring temperature also resulted in an increase in cooling rate ( $CR_{\text{Liq}}$ ) of the molten metal above liquidus, due to the same temperature of the mold wall, as seen in Fig. 3. The increased  $CR_{\text{Liq}}$  causes an increase in driving force for the critical nuclei growing into the nuclei. Thus, it shows that even if there is some re-melting or destruction of the active clusters with a high thermal input, the major reason for the decrease in the average  $\alpha$ -Mg grain size must be the co-effect of the increase in number of the active atom clusters and the cooling rate of the molten metal above liquidus, when the pouring temperature increased to 780 °C. In general, the effective number of the critical nuclei decreased with the increase in pouring temperature below 750 °C, but increased with further increase in pouring temperature up to 780 °C. As a result, the average  $\alpha$ -Mg grain size increased and subsequently decreased.

The result in the present study is different from that in Ref. [21], which reported that nucleation undercooling could affect the average grain size directly regarding the influence of the cooling rate and refiner/modifier on the solidification of Al–Si alloys. Considering the combining effect of the re-melting of the critical nucleus, the structure of the active atom clusters and the cooling rate (CR) on the nucleation and growth of the primary phase in the solidification mentioned above, it is worth noting that the characteristic parameters nucleation undercooling and nucleation time cannot be used to predict the nucleation or the average grain size directly any more, especially when the pouring temperature is changed in the solidification process.

### 4.3 Morphology

Due to the same chemical composition, all alloys had a typical solidification microstructure, with the equiaxed  $\alpha$ -Mg matrix and the eutectic phase along the grain boundaries. However, the morphology of the eutectic compounds transformed from a continuous network into a separated state (Fig. 9(a) and Fig. 11(a)) and subsequently into an island-like block (Fig. 9(d) and Fig. 11(c)). The size of the eutectic compounds increased, and some rod-like  $\beta$ -Mg<sub>24</sub>RE<sub>5</sub> particles appeared in the eutectic phase with the increase in the pouring temperature.

It was shown that the cooling rate decreased from 2.65 °C/s to 2.25 °C/s in Fig. 8, and the solidus increased with the decrease in the cooling rate in Table 4, with the pouring temperature increasing from 680 °C to 780 °C. The decrease in the cooling rate reduced the possibility of the grain growth, but increased the volume fraction of the remained liquid for the formation and growth of eutectic phase through decreasing the solidus until the end of the solidification. Additionally, the existing  $\alpha$ -Mg grains may more or less influence the morphology of the eutectic phase, especially with fine size and homogeneous distribution in the liquid. The eutectic reaction in the liquid will be therefore favored with the increase in the number of the  $\alpha$ -Mg grains, which plays as a promoter of the nucleation of the eutectic phase, considering the formation process directly starting on the surface of the solidified  $\alpha$ -Mg grain with its curvature. Totally, the cooling rate and the existing  $\alpha$ -Mg grain play roles together in the morphology of the eutectic compounds transformed from a continuous network into a separated state with the increase in the pouring temperature.

Solidification of these GW103K alloys begins with the crystallization of the  $\alpha$ -Mg phase, and then the composition of the remaining liquid shifts towards the eutectic composition where solidification proceeds by the eutectic reaction. After the formation of the  $\alpha$ -Mg

phase, more and more solute atoms transferred into the liquid through the solid–liquid interface with the decrease in the cooling rate. As a matter of fact, the solute content increased in the supersaturated liquid zone. During the eutectic reaction, the increased solute consistence increased the driving force and solute atoms for the formation and the growth of the  $\beta$ -Mg<sub>24</sub>RE<sub>5</sub> phase. Thus, the volume fraction of the  $\beta$ -Mg<sub>24</sub>RE<sub>5</sub> phase increased, and rod-like  $\beta$ -Mg<sub>24</sub>RE<sub>5</sub> phase formed in the eutectic phase. Solute concentration occurred in the eutectic zone.

Some small pores appeared at point 3 in Fig. 9(a) at the lowest temperature of 680 °C, and some inclusions were at point 3 in Fig. 9(d) at the lowest temperature of 780 °C. Solidification shrinkage occurs as the liquid metal becomes a solid with high density [28]. On one hand, when the liquid metal was poured into the mold at the lowest pouring temperature of 680 °C, the volume fraction of the liquid decreased with nucleation and growth of the  $\alpha$ -Mg phase. On the other hand, the fluidity of the molten metal decreased fastest [24], due to the highest cooling rate. The two factors above can limit or cut off the feeding process in the solidification. Thus, small pores formed with the further solidification shrinkage of the remaining molten metal. In the casting industry, a high pouring temperature has been usually chosen for forming some extremely complex castings to increase the fluidity of the liquid metal [7,26]. But it also causes re-oxidation of the melting magnesium (Fig. 9(d)) during the holding or the pouring process of the liquid magnesium, based on the factor that the oxidation rate is directly related to the temperature of molten magnesium alloy [27,32]. For sand-cast GW103K alloys, the lowest pouring temperature of 680 °C can refine the average grain size of  $\alpha$ -Mg but cause significant micro-porosities, while the highest pouring temperature of 780 °C can also refine the average grain size of  $\alpha$ -Mg but cause evident oxidation inclusion, besides the solute concentration.

#### 4.4 Strengthening mechanism and fracture surface

A fine equiaxed grain size in castings leads to a homogenized microstructure and improves the mechanical properties [33]. Figure 13 shows the relationship between  $d^{-1/2}$  and the YS of the alloy. Considering Hall–Petch strengthening mechanism, a good linear relationship indicated that the average  $\alpha$ -Mg grain size still played a main role in YS, when the pouring temperature was between 720 °C and 780 °C.

However, average grain sizes of the alloy poured at 680 °C and 780 °C were approximately the same and smaller than others. But the YS kept on increasing with increase in the pouring temperature, which implied that the grain size was the factor affecting the YS of the studied alloy. Meanwhile, besides the grain size and the

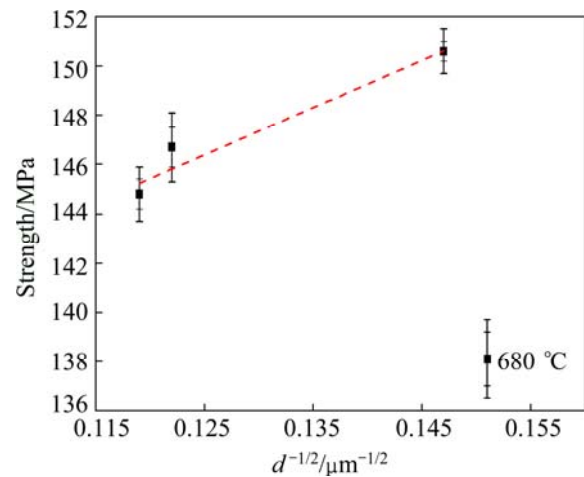
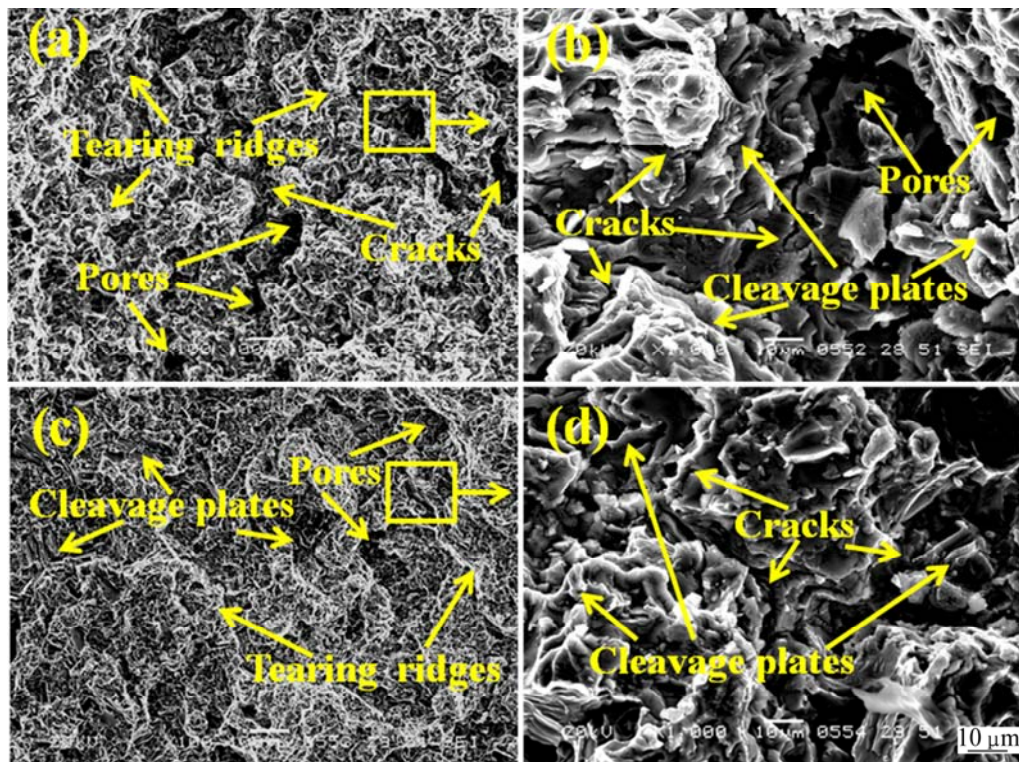


Fig. 13 Relationship between yield strength and average grain size of  $\alpha$ -Mg for sand-cast GW103K alloys

second phase, the amount of micro-porosity can also have an influence on the mechanical performance of the as-cast metals [34]. It was found that micro-porosity existed in specimens of as-cast Mg alloys poured at a low temperature, which was just a little higher than the liquidus of the Mg alloys [4,35]. The low pouring temperature caused it more prone to shrinkage voids or micro-porosities. It can be implied that the micro-porosity might decrease the YS, due to the fact that the YS of the alloy poured at 680 °C was out of the linear relationship in Fig. 13 (see pores in Figs. 9(a) and 14(a)). The re-oxidation inclusion can weaken mechanical properties of the alloy. This is the reason why both UTS and El of the alloy poured at 780 °C were lower than those of the alloy poured at 750 °C, considering the grain size effect.

The proper morphology of the second phase can increase the YS of sand-cast GW103K alloys [7], more or less, the change in morphology of the eutectic compound and the  $\beta$ -Mg<sub>24</sub>RE<sub>5</sub> particles could affect the mechanical properties of the sand-cast alloy. Additionally, the potential micro-porosity may also weaken the mechanical properties of the studied alloy caused by high pouring temperature, regarding to the factor that the re-oxidation inclusion can increase the micro-porosity of the as-cast alloy providing the needed nucleation sites for porosity formation [36]. But lacking of the direct evidence makes this influence weak, due to the observation results of the optical microstructure in Fig. 9(d), the microstructure in Fig. 11(c) and fracture surface of the sand-cast GW103K alloy in Fig. 14.

It is confirmed that some pores appear in Fig. 14(a). These pores are probably separated into two parts. Some are the original micro-porosities caused by the solidification shrinkage; others are the fresh micro-porosities formed during the tensile deformation



**Fig. 14** Typical SEM images at two magnifications showing fracture surfaces of sand-cast GW103K alloys at different pouring temperatures: (a, b) 680 °C; (c, d) 780 °C

process. Cracks were found inside the eutectic compound along the grain boundaries in Fig. 14(b). During the deformation process, damage was firstly produced by the fragmentation of eutectic particles or these micro-porosities, where a lot of tear ridges appeared. These tear ridges tend to merge in the direction of crack growth, and can be used to identify local crack initiation and growth events. Thus, the crack began forming or growing along the continuous network eutectic phase or in the  $\alpha$ -Mg grains. The quasi-cleavage crack plus dimple-like fracture is supposed to be the fracture surface type of the sand-cast GW103K alloy poured at 680 °C.

Fewer pores are observed on the fracture surface of the alloy poured at the highest temperature in Fig. 14(c), compared with the results in Fig. 14(a). Besides these pores, lots of cracks were observed on the tensile fracture surface of the sand-cast alloy in Fig. 14(c). It was reported that the micro-crack progressed across the  $\alpha$ -Mg grains as the cleavage fractured, after it formed inside the  $\alpha$ -Mg grains [7]. In the present study, the eutectic compounds became more and more separated with the increase in pouring temperature, transforming from a continuous network into a separated state (Figs. 9(a) and 11(a)) and subsequently into island-like blocks (Figs. 9(d) and 11(c)). These separated island-shaped eutectic compound blocks formed and solute

concentration zone increased in the  $\alpha$ -Mg grains with the increase in pouring temperature, both of which can make the crack form and grow more easily. The cleavage fracture will occur at the interface between the eutectic phase and the Mg matrix, due to the high mismatch between magnesium and solute atoms [35]. And this effect would probably be enhanced by solute concentration. The forming process of these cracks can be explained: firstly, the cracks form easily by the break of the  $\alpha$ -Mg grains, as seen in Fig. 14(c). Then, lots of small cleavage planes are left on the fracture surface (Fig. 14(d)). As the soft  $\alpha$ -Mg matrix interior has little resistance to the crack propagation, these cracks travel in a transgranular way after the formation, and some pores consisted of the hard eutectic particles are left at grain boundaries.

In general, the typical fracture surface mode of sand-cast GW103K alloy is transgranular fracture plus dimple-like fracture. With increase in pouring temperature, the fracture surface transforms from quasi-cleavage crack into transgranular fracture, including the micro-porosity.

## 5 Conclusions

1) The increase in pouring temperature can increase the nucleation temperature of the  $\alpha$ -Mg phase and the

solidus temperature, but decrease the cooling rate. The nucleation undercooling of the  $\alpha$ -Mg phase increased from 2.3 to 6.3 °C.

2) The average size of  $\alpha$ -Mg grain increased from 44  $\mu\text{m}$  to 71  $\mu\text{m}$ , but then decreased to 46  $\mu\text{m}$ . The morphology of the eutectic compound transformed from a continuous network into an island-like block with increasing volume fraction of eutectic compounds.

3) The survival number of critical nuclei was supposed to be the main reason for the grain refinement affected by the combining effect of the re-melting and the cooling rate of the molten metal above liquidus.

4) YS increased from 138 to 151 MPa, and UTS increased from 186 to 197 MPa. The alloy poured at 750 °C had the optimal combining strength and ductility. The typical fracture surface mode of the alloy is transgranular fracture plus dimple-like fracture.

## References

- [1] WANG Yin-xing, ZENG Xiao-qin, DING Wen-jiang. Effect of Al-4Ti-5B master alloy on the grain refinement of AZ31 magnesium alloy [J]. *Script Materials* 2006, 54, 269–273.
- [2] CAO Hai-ping, WESSÉN M. Effect of microstructure on mechanical properties of as-cast Mg-Al alloys [J]. *Metallurgical and Materials Transactions A*, 2004, 35 (1): 309–319.
- [3] MA Qian, DAS A. Grain refinement of magnesium alloys by zirconium: Formation of equiaxed grains [J]. *Script Materials*, 2006, 54(5): 881–886.
- [4] STJOHN D H, QIAN M A, EASTON M A, CAO P, HILDEBRAND Z. Grain refinement of magnesium alloys [J]. *Metallurgical and Materials Transactions A*, 2005, 36(7): 1669–1679.
- [5] LIU Zhi-jie, WU Guo-hua, LIU Wen-cai, PANG Song, DING Wen-jiang. Microstructure, mechanical properties and fracture behavior of peak-aged Mg-4Y-2Nd-1Gd alloys under different aging conditions [J]. *Materials Science and Engineering A*, 2013, 561: 303–311.
- [6] LI Zhen-ming, LUO A, WANG Q, PENG Li-ming, FU Peng-huai, WU Guo-hua. Effects of grain size and heat treatment on the tensile properties of Mg-3Nd-0.2Zn (wt.%) magnesium alloys [J]. *Materials Science and Engineering A*, 2013, 564: 450–460.
- [7] PANG Song, WU Guo-hua, LIU Wen-cai, SUN Ming, ZHANG Yang, LIU Zhi-jie, DING Wen-jiang. Effect of cooling rate on the microstructure and mechanical properties of sand-casting Mg-10Gd-3Y-0.5Zr magnesium alloy [J]. *Materials Science and Engineering A*, 2013, 562(1): 152–160.
- [8] HONMA T, OHKUBO T, KAMADO S, HONO K. Effect of Zn additions on the age-hardening of Mg-2.0Gd-1.2Y-0.2Zr alloys [J]. *Acta Materialia*, 2007, 55(12): 4137–4150.
- [9] ZHOU Hao, YE Bing, WANG Qu-dong, GUO Wei. Uniform fine microstructure and random texture of Mg-9.8Gd-2.7Y-0.4Zr magnesium alloy processed by repeated-upsetting deformation [J]. *Materials Letters*, 2012, 83: 175–178.
- [10] LIU Wen-cai, DONG Jie, SONG Xiang, BELNOUE J, HOFMANN F, DING Wen-jiang, KORSUNSKY A. Effect of microstructures and texture development on tensile properties of Mg-10Gd-3Y alloy [J]. *Materials Science and Engineering A*, 2011, 528(6): 2250–2258.
- [11] FLEMINGS M. *Solidification Processing* [M]. USA, New York: McGraw-Hill, 1974: 73–74.
- [12] CAO Peng, MA Qian, STJOHN D. Mechanism for grain refinement of magnesium alloys by superheating [J]. *Script Materials*, 2007, 56(7): 633–636.
- [13] TINER N. Superheating of magnesium alloys [J]. *Transaction of American Institute of Mining, Metallurgical, and Petroleum Engineers*, 1945, 161: 242–264.
- [14] ACHENBACH K, NIPPER H, PIWOWARSKY E. Contribution to the question of melting practice for cast magnesium alloys [J]. *Die Giesserei*, 1939, 26: 621–623.
- [15] MONDOLFO L F, BARLOCK J G. Effect of superheating on structure of some aluminum alloys [J]. *Metallurgical Transactions B*, 1975, 6(4): 565–572.
- [16] RAMACHANDRAN T R, SHARMA P K, BALASUBRAMANIAN K. Grain refinement of light alloys [C]//*Proceedings of the 68th WFC—World Foundry Congress*. India, Chennai: Institute of Indian Foundrymen, 2008: 189–193.
- [17] WANG J, MENG J, ZHANG D. Effect of Y for enhanced age hardening response and mechanical properties of Mg-Gd-Y-Zr alloys [J]. *Materials Science and Engineering A*, 2007, 456(1–2): 78–84.
- [18] MIZER D, CLARK J. The magnesium-rich region of the magnesium-yttrium phase diagram [J]. *Transactions of the Metallurgical Society of AIME*, 1961, 221: 207–208.
- [19] MIZER D, PETERS B. A study of precipitation at elevated temperature in a Mg-8.7pct Y alloys [J]. *Metallurgical and Materials Transactions B*, 1972, 3(12): 3262–3264.
- [20] KAMADO Y, KOJIMA R, NINOMIYA R. Aging characteristics and high temperature tensile properties of magnesium alloys containing heavy rare earth elements [C]//*Proceedings of the 3rd International Magnesium Conference*. United Kingdom: Manchester, 1996: 327–342.
- [21] SHABESTARI S G, GHODRAT S. Assessment of modification and formation of intermetallic compounds in aluminum alloy using thermal analysis [J]. *Materials Science and Engineering A*, 2007, 467(1): 150–158.
- [22] GOURLAY C M, DAHLE A K. Dilatant shear bands in solidifying metals [J]. *Nature*, 2007, 445(7123): 70–73.
- [23] GÜNDÜZ S. Effect of chemical composition, martensite volume fraction and tempering on tensile behaviour of dual phase steels [J]. *Materials Letters*, 2009, 63(27): 2381–2383.
- [24] QIAN Ma, STJOHN D H, FROST M T. Characteristic zirconium-rich coring structures in Mg-Zr alloys [J]. *Script Materials*, 2002, 46: 649–654.
- [25] CHEN Zhong-wei, JIE Wan-qi, ZHANG Rui-jie. Superheat treatment of Al-7Si-0.55 Mg alloy melt [J]. *Materials Letters*, 2005, 59(17): 2183–2185.
- [26] WILFRIED K, FISHER D J. *Fundamentals of Solidification* [M]. Switzerland, Laubisrutistr: Trans Tech Publications Ltd, 1986: 247.
- [27] CHRISTIAN J. *The theory of transformations in metal and alloys* [M]. Oxford: Pergamon, 1975: 450.
- [28] CHALMERS B. *Principles of Solidification* [M]. New York, USA: : Wiley, 1964: 92.
- [29] POOLE P, GRANDE T, ANGELL C, MCMILLAN P. Polymorphic phase transitions in liquids and glasses [J]. *Science*, 1997, 275: 322–323.
- [30] SHEN Rong-rong, ZU Fang-qiu, LI Qiang, XI Yun, LI Xian-fen, DING Guo-hua, LIU Hai-ming. Study on temperature dependence of resistivity in liquid In-Sn alloy [J]. *Physica Scripta*, 2006, 73(2): 184–187.
- [31] LL'INSKII A, KABAN I, KOVAL Y, HOYER W, SLYUSARENKO S. On thermodynamic properties and atomic structure of amorphous and liquid alloys [J]. *Journal of Non-crystalline Solids*, 2004, 345: 251–255.
- [32] PANG Song, WU Guo-hua, SUN Ming, DAI Ji-chun, ZHANG Yang, DING Wen-jiang. Present status and prospect on protective gas used

- in melting of magnesium alloy [J]. China Foundry, 2011, 60(3): 259–264.
- [33] CHANDRASHEKAR T, MURALIDHARA M K, KASHYAP K T, RAO P R. Effect of growth restricting factor on grain refinement of aluminum alloys [J]. The International Journal of Advanced Manufacturing Technology, 2009, 40(3–4): 234–241.
- [34] CAO H, WESSÉN M. Effect of microstructure on mechanical properties of as-cast Mg–Al alloys [J]. Metallurgical and Materials Transactions A, 2004, 35: 309–319.
- [35] TAMURA Y, KONO N, MOTEGI T, SATO E. Grain refining mechanism and casting structure of Mg–Zr alloy [J]. Japan Institute of Light Metals, 1998, 48(4): 185–189.
- [36] MONROE R. Porosity in castings [J]. Transactions of American Foundry Society, 2005, 5: 1–28.

## 浇注温度对砂型铸造 Mg–10Gd–3Y–0.4Zr 合金 凝固行为、组织与性能的影响

庞松<sup>1,2</sup>, 吴国华<sup>1</sup>, 刘文才<sup>1</sup>, 张亮<sup>1</sup>, 张扬<sup>1</sup>, Hans CONRAD<sup>2</sup>, 丁文江<sup>1</sup>

1. 上海交通大学 轻合金精密成型国家工程研究中心与金属基复合材料国家重点实验室, 上海 200240;
2. Department of Materials Science and Engineering, North Carolina State University, Raleigh, NC 27695-7907, USA

**摘要:** 研究砂型铸造过程中浇注温度(680~780 °C)对 Mg–10Gd–3Y–0.4Zr 合金凝固行为、组织与性能的影响。结果表明: 随着浇注温度从 680 °C 先提高至 750 °C 再提高至 780 °C,  $\alpha$ -Mg 的形核过冷度从 2.3 °C 提高到 6.3 °C 后不再提高;  $\alpha$ -Mg 的平均晶粒尺寸先由 44  $\mu\text{m}$  增加至 71  $\mu\text{m}$  而后减小到 46  $\mu\text{m}$ ; 共晶组织先由网格状转变为不连续的块状继而转变为大块的岛状;  $\beta$ -Mg<sub>24</sub>RE<sub>5</sub> 相的体积分数增加, 由颗粒状转变为短棒状; 溶质富集的现象变得更加明显; 合金的屈服强度由 138 MPa 提高至 151 MPa, 抗拉强度由 186 MPa 提高至 197 MPa。750 °C 浇注的合金具有最佳的强度与延展性。断口形貌特征由准解理断裂转变为穿晶韧性断裂, 并伴随着不同程度的缩松与氧化夹杂等铸造缺陷。相对于铸造缺陷、共晶组织以及溶质富集,  $\alpha$ -Mg 的晶粒尺寸是砂型铸造 Mg–10Gd–3Y–0.4Zr 合金屈服强度最主要的影响因素。

**关键词:** 砂型铸造; 镁合金; 凝固; 组织; 力学性能

(Edited by Xiang-qun LI)